In-beam gamma ray and conversion electron study of ^{250}Fm

J. E. Bastin,[1] R.-D. Herzberg,[1] P. A. Butler,[1] G. D. Jones,[1] R. D. Page,[1] D. G. Jenkins,[1,*] N. Amzal,[1] P. M. T. Brew,[1] N. J. Hammond,[1] R. D. Humphreys,[1] P. J. C. Ikin,[1] T. Page,[1] P. T. Greenlees,[2] P. M. Jones,[2] R. Julin,[2] S. Juutinen,[2] H. Kankaanpää,[2] A. Keenan,[2] H. Kettunen,[2] P. Kuusiniemi,[2] M. Leino,[2] A. P. Leppänen,[2] M. Muikku,[2,†] P. Nieminen,[2,‡] P. Rahkila,[2] C. Scholey,[2] J. Uusitalo,[2] E. Bouchez,[3] A. Chatillon,[3] A. Hürstel,[3] W. Korten,[3] Y. Le Coz,[3] Ch. Theisen,[3] D. Ackermann,[4] J. Gerl,[4] K. Helariutta,[4] F. P. Hessberger,[4] Ch. Schlegel,[4] H. J. Wollerscheim,[4] M. Lach,[5] A. Maj,[5] W. Meczynski,[5] J. Styczen,[5] T. L. Khoo,[6] C. J. Lister,[6] A. V. Afanasjev,[7,8] H. J. Maier,[9] P. Reiter,[10] P. Bednarczyc,[11] K. Eskola,[12] and K. Hauschild[13]

[1]*Oliver Lodge Laboratory, University of Liverpool, Liverpool L69 7ZE, United Kingdom*
[2]*Department of Physics, P.O. Box 35 (YFL), FIN-40014, University of Jyväskylä, Finland*
[3]*DAPNIA/SPhN CEA Saclay, F-91191 Gif/Yvette Cedex, France*
[4]*Gesellschaft für Schwerionenforschung, D-64291 Darmstadt, Germany*
[5]*The Henryk Niewodniczanski Institute of Nuclear Physics, PL-31-342, Krakow, Poland*
[6]*Physics Division, Argonne National Laboratory, Argonne, Illinois 60439, USA*
[7]*Department of Physics, University of Notre Dame, Notre Dame, Indiana 46556, USA*
[8]*Institute of Solid State Physics, University of Latvia, LV 2169 Salaspils, Latvia*
[9]*Ludwig Maximilians Universität, D-80539, München, Germany*
[10]*Institut für Kernphysik, Universität zu Köln, D-50937 Köln, Germany*
[11]*Institut de Recherches Subatomiques, F-67037, Strasbourg, France*
[12]*Department of Physics, University of Helsinki, FIN-00014, Helsinki, Finland*
[13]*CNSM Orsay, IN2P3/CNRS, F-91405 Orsay Campus, France*

(Received 7 July 2005; published 9 February 2006)

We report on a set of in-beam studies of excited states in ^{250}Fm. We detected prompt γ rays by using the JUROSPHERE IV array and conversion electrons by using the SACRED spectrometer. Both devices were used in conjunction with the RITU gas-filled recoil separator located at the University of Jyväskylä. ^{250}Fm nuclei were produced through the ^{204}Hg(^{48}Ca,2n)^{250}Fm fusion-evaporation reaction. An experimental excitation function gave a maximum reaction cross section of (980 ± 160) nb at an energy of 209 MeV in the center of the target. Tagging techniques were employed, and a number of $E2$ transitions were observed that connected the ground-state band levels from spin 4^+ up to 18^+. The highly converted $4^+ \rightarrow 2^+$ transition is observed only by use of conversion electron spectroscopy. The observed ground-state band transitions indicate a rotational structure. We deduce a quadrupole deformation parameter of $\beta_2 = 0.28 \pm 0.02$. A low-energy background of apparent nuclear origin is observed in conversion electrons and postulated to arise from the decay of high-K bands. The half-life of ^{250}Fm is measured to be 30.4 ± 1.5 min.

DOI: 10.1103/PhysRevC.73.024308 PACS number(s): 27.90.+b, 23.20.Lv, 23.20.Nx, 29.30.Dn

I. INTRODUCTION

The question of the location and nature of the next spherical shell closures beyond lead has been a driving force behind nuclear structure physics over the past four decades. After the first predictions of shell stabilization [1–3], a variety of theoretical approaches was used to predict the location of the shell gaps.

Currently three major predictions are under discussion. The macroscopic-microscopic approaches predict a doubly magic shell closure at $Z = 114, N = 184$ [3–10]. Many parametrizations of nonrelativistic self-consistent models predict it at $Z = 126, N = 184$ [11,12]. However, in a number of parametrizations no double shell closure is seen and a large proton gap appears at $Z = 120$. In relativistic mean-field (RMF) models, a double shell closure at $Z = 120, N = 172$, is favored [11–15].

Nuclei close to this region have been successfully produced, albeit at the level of a few atoms. At GSI (Gesellschaft für Schwerionenforschung), the elements up to $Z = 112$ have been produced and unambigously identified by means of α-decay chains ending in well-known lighter isotopes [16]. At Dubna several isotopes of elements 114 [17], 115 [18], and 116 [19] have been reported, and recently element 113 was reported from RIKEN [20]. Although proton number 116 has thus been reached, the isotopes produced were still rather neutron deficient compared with the most stable neutron configuration with $N = 184$ predicted by the macroscopic-microscopic method. A further means of studying the evolution of single-particle states in this region is the study of the α decays of odd-mass nuclei. These decays populate excited states in the daughter nuclei. Because

*Permanent address: Department of Physics, University of York, Heslington, York, Y01 5DD, UK.
†Permanent address: Radiation and Nuclear Safety Authority, P. O. Box 14, FIN-00881 Helsinki, Finland.
‡Current address: Department of Nuclear Physics, Australian National University, Canberra, ACT 0200, Australia.

α decays between identical configurations are favored, this allows a mapping of the single-particle orbitals close to the Fermi surface [21,22].

A different approach is to study the deformed lighter nuclei around $^{254}_{102}No_{152}$. There we find that, because of the large deformation, the Nilsson orbitals close to the Fermi surface are derived from spherical single-particle states that lie close to the Fermi level in much heavier systems with $Z = 114$–126. Certain experimental observables allow us to select the effective forces that are best suited to the description of superheavy nuclei. The rotational properties of the nuclei in the $A \sim 250$ mass region are expected to be sensitive to a number of high-j orbitals emerging from the spherical subshells active in the vicinity of the predicted shell closures.

The feasibility of in-beam studies of rotational structures in superheavy nuclei has only recently been demonstrated in ^{254}No [23–26], which can be produced at a relatively large cross section of 2–3 μb. The setup at the University of Jyväskylä has since been steadily improved. The study of ^{252}No was possible at a cross section of only 220 nb [27]. In both No nuclei, the ground-state band was observed up to spin $I = 20^+$, close to the expected upbend.

The aim of the present study was to establish the ground-state band in ^{250}Fm to comparable spin. Two experiments were performed: one using γ ray spectroscopy with JUROSPHERE IV and the other studying conversion electrons with the Silicon Array for Conversion Electron Detection (SACRED) spectrometer. Both devices were coupled to the Recoil Ion Transport Unit (RITU) gas-filled separator. In Sec. II we discuss both experimental setups; the experimental findings for both experiments are presented in Sec. III. We have tried to keep the discussion of the experiments separate as far as possible. Owing to the complementary nature of the two probes this could not always be achieved. Section V compares the observed ground-state band with calculations done within the framework of the cranked relativistic Hartree-Bogoliubov (CRHB) theory. Finally, the conclusions are given.

II. EXPERIMENTAL DETAILS

A. γ-ray spectroscopy

The experiment was performed at the University of Jyväskylä Accelerator Laboratory; the JUROSPHERE IV [28] array was used in conjunction with the RITU gas-filled recoil separator [29,30]. ^{250}Fm nuclei were produced by means of the reaction ^{204}Hg(^{48}Ca,2n)^{250}Fm at a beam energy of 210 MeV in the center of the target. Evaporation residues were separated from the beam by magnetic rigidity before implantation in a 16-strip position-sensitive silicon detector (PSSD) at the RITU focal plane. The beam energy was chosen following an experimentally performed excitation function guided by the HIVAP code; see Fig. 1. The measurements indicated a maximum in the reaction cross section at 209 MeV.

We ran the experiment at the slightly higher value of 210 MeV in order to introduce more angular momentum into the system. A stack of two enriched ^{204}HgS targets [31,32], each of thickness 250 μg/cm^2 evaporated onto 14-μg/cm^2 carbon backing, was used. The targets were found to survive irradiation with an 8-pnA beam for the 1-week experimental

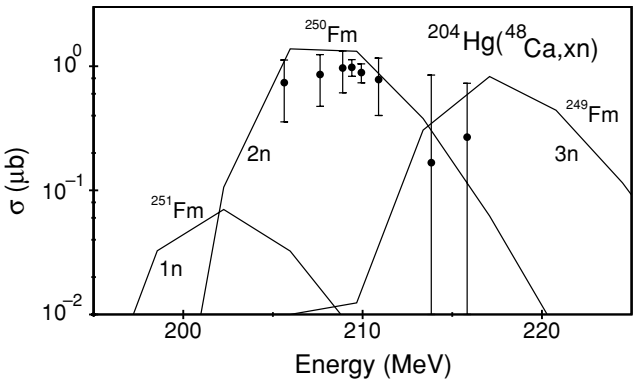

FIG. 1. Predictions of the HIVAP code (solid lines) and experimentaly measured reaction cross sections (filled circles).

period. The presence of the 1-mbar He RITU fill gas in the target region aided target cooling and removed the need for a target wheel. Tests with natural HgS targets of similar construction showed rapid deterioration with beam intensities above 15 pnA. It is worth noting that, when the used target was examined several months after the experiment, the HgS material under the beam spot was found to have evaporated in storage.

The PSSD allowed the recording of position, energy, and time information for both recoil implantation and subsequent α-decay events. Two sets of electronics with different gain ranges were required for retaining good resolution for the α-decay peaks and extending the energy range to cover the implanted recoils. Discrimination of α-decay and implantation events was greatly helped by the presence of a multiwire proportional avalanche counter (MWPC) upstream from the PSSD. Only events in anticoincidence to the gas detector were recorded as α decays. This resulted in very clean α-decay spectra. The region of interest of the resulting total α spectrum is shown in Fig. 2. In the inset we show the region between

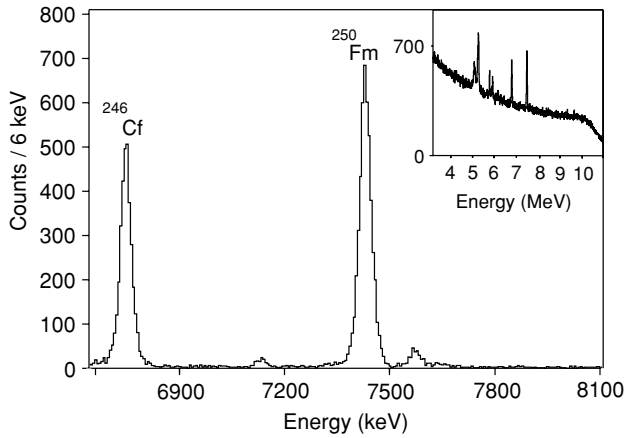

FIG. 2. Total α-decay spectrum obtained from the 16-strip silicon detector at the RITU focal plane. We remove recoils by demanding anticoincidence with gas detector events. The characteristic 7.436-MeV α-decay peak of ^{250}Fm is observed together with the decay peak of the daughter nucleus ^{246}Cf. In the inset we show the overlap between the implantation distribution and the region containing the α-decay peaks.

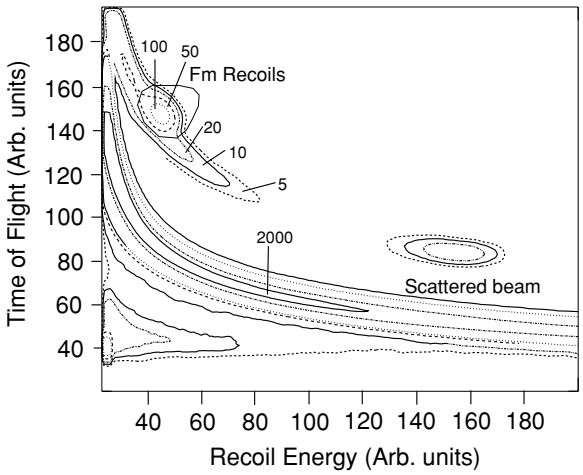

FIG. 3. The time-of-flight matrix is a two-dimensional histogram produced by the plotting of the time of flight against implantation energy. A polygonal gate (solid curve) was set on recoils of interest and target position events that were in delayed coincidence with such recoils selected.

3 and 11 MeV of the raw PSSD spectrum. The overlap between the distribution of implantation events and the region containing the α-decay peaks is clearly seen.

For this experiment the JUROSPHERE IV array was used in a configuration of 22 Compton-suppressed germanium detectors with a photopeak efficiency of 1.1%. To pull the ^{250}Fm γ rays from the comparatively large background, a recoil-γ coincidence technique was used. The velocity of recoils was measured from their time of flight between the gas and implantation detectors. Figure 3 shows the resulting matrix of time of flight against implantation energy. A polygonal gate was set to select the ^{250}Fm evaporation residues. The gate is indicated in Fig. 3.

The assignment of transitions to ^{250}Fm was confirmed by use of the method of recoil decay tagging (RDT) [33,34]. If a characteristic ^{250}Fm α decay is observed at the same position and within three half-lives of the detection of a recoil, then that recoil is assumed to be ^{250}Fm and associated γ rays incremented into a spectrum. Figure 4 shows the γ rays gated on ^{250}Fm recoils in the upper panel and an RDT spectrum requiring a subsequent α decay in the lower panel.

B. Conversion electron spectroscopy

Conversion electron data were obtained with the SACRED spectrometer [35] in conjunction with the RITU gas-filled recoil separator. The SACRED device consists of a circular 25-element silicon array 27.5 mm in diameter situated 550 mm upstream of the target position. The array is built on a single Si p-i-n wafer 500 μm in thickness. Electrons are transported from the target position to the array by means of a 0.3-T solenoidal field. The field is generated by four conventional water-cooled solenoids. The array is positioned in an almost collinear geometry with the beam and solenoidal axes making an angle of 2.5°. This allows the array to be coupled to the recoil separator and offers the advantages of

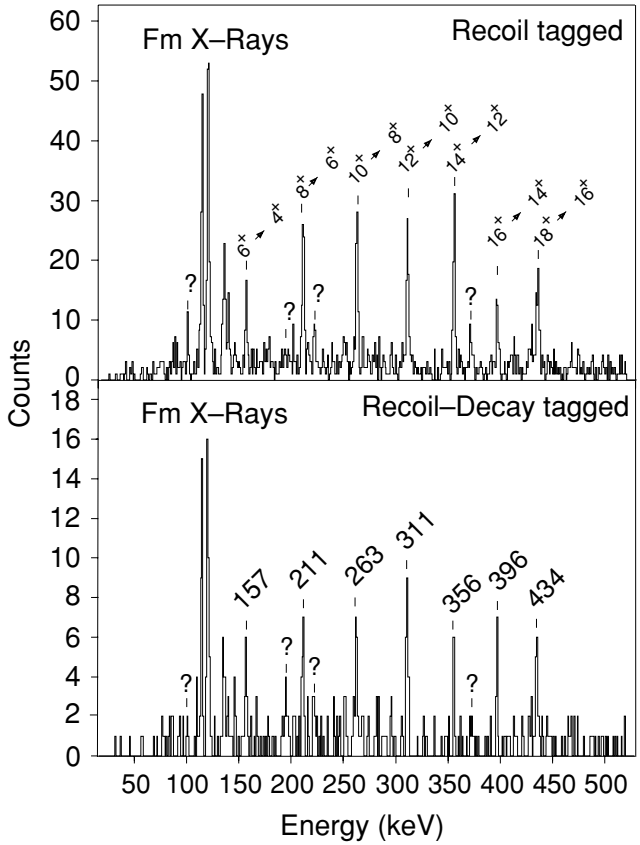

FIG. 4. Upper panel: Recoil tagged spectrum we produced by demanding γ rays in coincidence with recoils that pass the polygonal gate shown in Fig. 2. Lower panel: Recoil decay tagged spectrum we produced by demanding coincidence with recoils detected in pixels in which a characteristic ^{250}Fm α decay is detected within three half-lives (90 mins) of the implantation.

reduced Doppler broadening and reduced δ-electron yield in the backward direction. The SACRED array is separated from the RITU helium fill gas by two 60-μg/cm^2 carbon foils with differentially pumped intermediate volume. The location of the foils between the target and array allows the gas to cool the targets. The δ-electron background created by collisions between beam particles and target is suppressed by a -40-kV electrostatic barrier. In this experiment the population of high-spin states was not of great importance as the higher-lying ground-state band transitions are not strongly converted and could not be populated with sufficient statistics. A beam of 209-MeV energy at the center of the target, the maximum of the experimentally determined excitation function, was therefore chosen to irradiate a single 260-μg/cm^2 ^{204}HgS target with 14 μg/cm^2 of carbon backing. The average beam intensity was 2.1 pnA, and a total of 2664 ^{250}Fm α decays were detected during the 7-day experimental period. As with the γ-ray experiment, transitions were identified primarily by recoil-electron coincidence, and the RDT method was used to confirm the assignment of transitions to ^{250}Fm. In the γ-ray experiment, the two-dimensional gate set on the time-of-flight versus implantation energy matrix was chosen so as to obtain the best statistics while keeping the spectra as clean as possible.

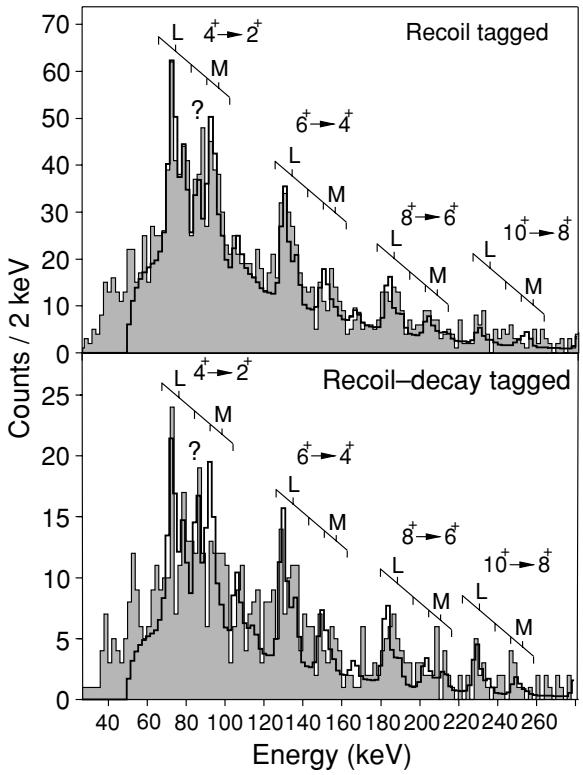

FIG. 5. Recoil and recoil decay tagged electron spectra with a 2 keV per channel dispersion. The experimental spectra are shaded gray. The solid lines are best fits consistent with the transition energies of the observed γ rays and the energy dependence of the efficiency of the SACRED device.

It should be noted that, in the conversion electron experiment, the placing of gates on regions of the matrix corresponding to recoils other than ^{250}Fm produced spectra containing a negligible number of counts. It was thus found that the best electron spectra were produced with a considerably wider gate than was used in the γ-ray experiment.

A series of conversion electron lines is seen corresponding to transitions from spin $4^+ \rightarrow 2^+$ up to $10^+ \rightarrow 8^+$, each with components arising from conversions with electrons from each of the atomic shells. The energy resolution of the SACRED spectrometer, which is dominated by the 3-keV intrinsic resolution of each of the detector pixels, allowed the resolution of three separate components, one arising from conversions with $L_{\rm I}$ and $L_{\rm II}$ electrons, a second from $L_{\rm III}$ electrons, and a third arising from conversions with any M shell electron. Conversions with electrons in other shells have little impact on the spectra; they are, however, accounted for by the simulated spectra of Fig. 5.

III. RESULTS

A. Cross section

No experimental determination of the cross section of the ^{204}Hg(^{48}Ca,2n) reaction is given in the literature. The experimental setup is not ideal for an accurate determination of this cross section and suffers mainly from uncertainties in the transmission of the recoil separator. Nonetheless, such uncertainties will be reflected in the errors given, and we deduce an experimental value from our data. The small implantation depth of the ^{250}Fm evaporation residues resulted in the effective loss of all α particles emitted in the backward direction. An α-decay branch of greater than 90% has been reported [36]. In our calculations we assume an α-decay branch of exactly 90%. We deduce recoil numbers from observed α decays, taking into account the 50% detection efficiency and double checking against the number of recoils identified from the energy versus time-of-flight matrix. The latter is used only as a confirmation as the discrimination between recoils and scattered beam is not as clean as simply integrating the α-decay peak. The γ-ray experiment was run at 210 MeV with a total beam dose of 6.53×10^{15} ^{48}Ca ions incident upon a stack of two targets of total thickness 528 μg/cm^2. In the conversion electron experiment a beam energy of 209 MeV was used with a beam dose of 3.11×10^{15} ^{48}Ca ions on a single target of thickness of 259 μg/cm^2. At 210 MeV (209 MeV) we observed 4800 $\pm$ 70 (2664 $\pm$ 50) full-energy α decays during the experimental period. This corresponds to 10670 $\pm$ 160 (5920 $\pm$ 120) ^{250}Fm nuclei implanted in the PSSD. In view of the difficulties in accurately determining the separator efficiency η, we give the product of the measured reaction cross section and separator efficiency $\sigma\eta$. We find $\sigma\eta_{210} = (220 \pm 60)$ nb and $\sigma\eta_{209} = (245 \pm 40)$ nb. If one assumes the transmission efficiency of RITU to be 25%, the cross section can be deduced. We obtain a maximum reaction cross section of $\sigma_{\rm max} = (980 \pm 160)$ nb. These values together with the estimates found in the short runs of the excitation function are shown together with the results of the HIVAP calculation in Fig. 1.

B. Half-life

We determined the ^{250}Fm half-life by measuring the time between the arrival of each recoil in a PSSD pixel and its subsequent α decay (Fig. 6). Measurements of this type are complicated by the possibility of a second recoil arriving in the same pixel as the first and before the α decay occurs.

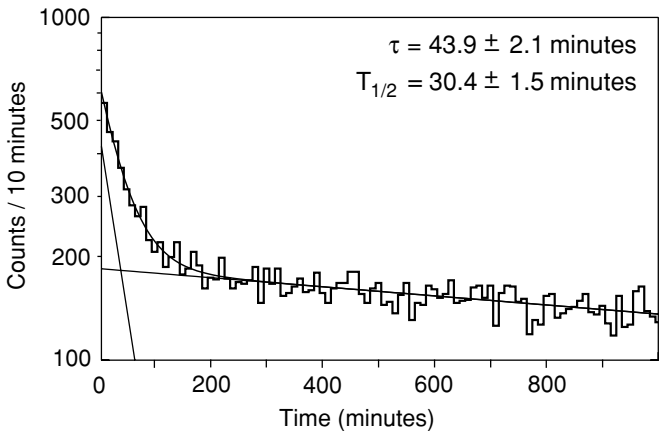

FIG. 6. The observed α-decay curve of ^{250}Fm. The double exponential fit used to extract the lifetime is shown together with a deconvolution of the two components of the fit.

TABLE I. Energies and intensities of ground-state band members measured with γ rays. $I_\gamma^\dagger$ and I_γ are intensities with and without correction for internal conversion, respectively. All intensities are normalized to the $14^+ \rightarrow 12^+$ transition.

Transition	E_γ	I_γ	$I_\gamma^\dagger$
$6^+ \rightarrow 4^+$	156.9 ± 0.1	30 ± 9	119 ± 34
$8^+ \rightarrow 6^+$	211.3 ± 0.1	70 ± 11	123 ± 20
$10^+ \rightarrow 8^+$	262.6 ± 0.2	86 ± 15	109 ± 19
$12^+ \rightarrow 10^+$	311.0 ± 0.2	75 ± 16	82 ± 18
$14^+ \rightarrow 12^+$	355.7 ± 0.1	100 ± 16	100 ± 16
$16^+ \rightarrow 14^+$	396.9 ± 0.2	50 ± 13	50 ± 13
$18^+ \rightarrow 16^+$	434.4 ± 0.2	46 ± 13	44 ± 11

The possibility of α decays occurring without full-energy deposition in the PSSD is also problematic. The former is of particular significance in ^{250}Fm owing to the long half-life. To account for this, the measured lifetime must be considered to have two components, a short component τ_{short} and a random component τ_{random}. The two components are related by $\tau_{\text{Fm}}^{-1} = \tau_{\text{short}}^{-1} - \tau_{\text{random}}^{-1}$ [37]. A double exponential fit to the data, correlated over 1000 min to obtain a good feel for the random background, was used to extract $\tau_{\text{short}} = (43.2 \pm 2.1)$ min and $\tau_{\text{random}} = (2970 \pm 120)$ min. This yields the ^{250}Fm lifetime as $\tau = (43.9 \pm 2.1)$ min and the corresponding half-life as $T_{\frac{1}{2}} = (30.4 \pm 1.5)$ min. The result is in agreement with the previously accepted value of $T_{\frac{1}{2}} = (33 \pm 3)$ min [38]. The data together with the fit and a deconvolution of its two components are shown in Fig. 6.

C. Ground-state band

In the γ-ray data a sequence of almost evenly spaced transitions is observed, indicating a rotational ground-state band. All strong transitions also show up in the RDT spectrum and clearly belong to ^{250}Fm; see Fig. 4. The energies and intensities of the strongly observed transitions were taken from the recoil gated spectra and are shown in Table I. Shown in Table II are the intensities of the ground-state band transitions seen in conversion electron spectra together with their corresponding deduced transition energies E_t. Here we find the energies of the lowest three transitions seen in the γ-ray spectra. In addition, the $4^+ \rightarrow 2^+$ transition is observed as the strongest line in the electron spectra.

A γ-ray peak is observed at 101 keV, consistent with the expected energy of the $4^+ \rightarrow 2^+$ transition. Its intensity, however, is too large to be accounted for by this highly converted ground-state band member alone. The expected peak area can be estimated from the intensity of the transition in the conversion electron spectra and the relative detection efficiencies of JUROSPHERE IV and SACRED. Its area should be about five counts, barely visible above background. The observed transition has 14 ± 5 counts and thus seems too large to stem just from the $4^+ \rightarrow 2^+$ transition. Whether a doublet exists at this energy or the observed intensity is due to a statistical fluke cannot be decided at the present level of statistics.

TABLE II. Deduced transition energies and intensities of ground-state band members measured with conversion electrons. Intensities are normalized to 100 for the $L_{\text{I+II}}$ component of the $4^+ \rightarrow 2^+$ transition

Transition	E_t	$I_{L_{\text{I+II}}}$	$I_{L_{\text{III}}}$	I_M
$4^+ \rightarrow 2^+$	100.0 ± 1.0	100 ± 21	47 ± 13	51 ± 12
$6^+ \rightarrow 4^+$	157.4 ± 1.0	42 ± 7	10 ± 4	16 ± 5
$8^+ \rightarrow 6^+$	211.0 ± 1.0	14 ± 4	8 ± 3	9 ± 4
$10^+ \rightarrow 8^+$	257.4 ± 2.0	9 ± 3	4 ± 2	6 ± 3

In the γ-ray spectra we observe small peaks at 195, 222, and 372 keV, which clearly do not belong to the ground-state band. Their presence in the RDT spectrum supports their assignment to ^{250}Fm. The peaks are labeled with question marks in Fig. 4. Note that the 101-keV ground-state band candidate is also labeled with a question mark owing to its unexplained intensity.

The available statistics allowed the construction of a γ-γ coincidence matrix. Although the statistics are at the limit of usefulness, coincidences at the single-count level on an extremely low background can nonetheless be used to demonstrate the mutual coincidence of the observed ground-state band transitions.

Shown in the upper panel of Fig. 7 is the total projection of the coincidence matrix constructed from recoil gated events only. The lower panel shows a gate sum produced by demanding that every γ ray incremented in the spectrum be in coincidence with at least one ground-state band transition or the Fm x rays.

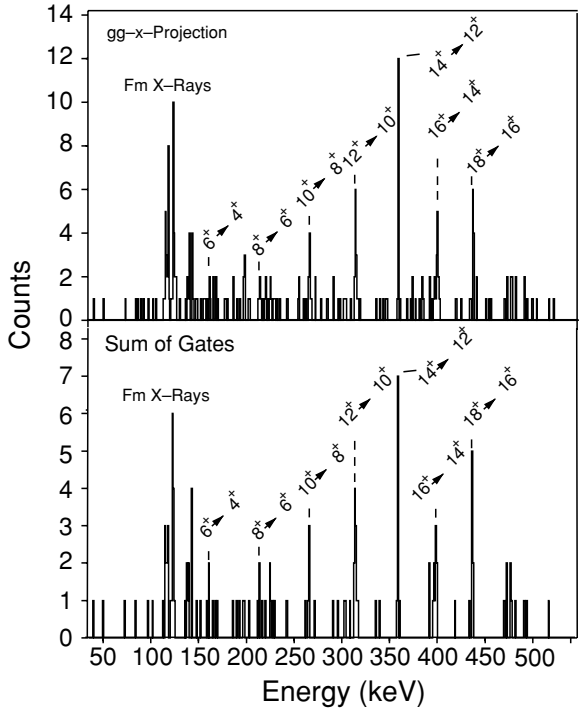

FIG. 7. Comparison of the γ-γ coincidence matrix total projection with a sum of gates set on ground-state band transitions in addition to the Fm x rays.

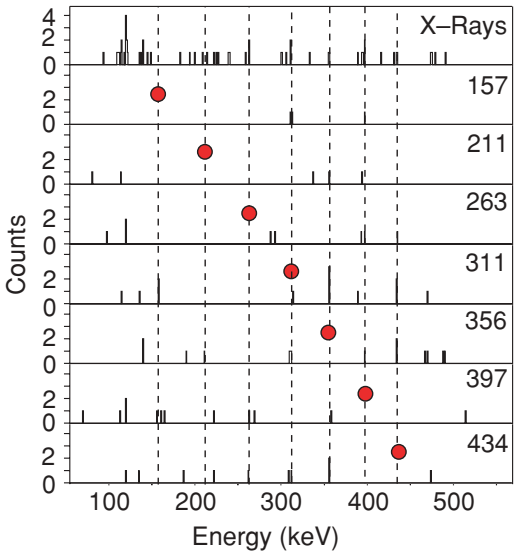

FIG. 8. (Color online) Comparison of gates set on ground-state band members. Indicated at the top-right-hand side of each panel is the transition on which the gate was set; in all cases the gate width was 5 keV. The dashed lines indicate the positions of ground-state band transitions, and filled circles mark the transition on which each spectrum is gated.

In the total projection we clearly see evidence of the unplaced transition at 195 keV. Shown in Fig. 8 is a comparison of the individual spectra gated on each of the ground-state band members and the Fm x rays. These spectra further demonstrate that the ground-state band transitions are in coincidence and, although the statistics obtained are at the limit of usefulness, serve to illustrate well that an in-depth coincidence analysis is tantalizingly feasible at the 1-μb level.

Shown in Fig. 9 is a comparison of a sum of gates set on ground-state band transitions [Fig. 9(a)] with gates set on the unplaced transitions [Figs. 9(b)–9(d)]. In the ground-state band

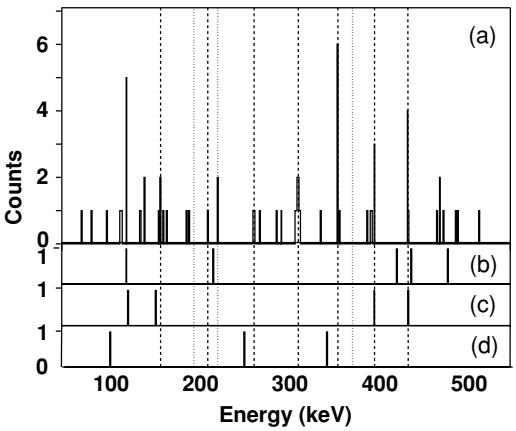

FIG. 9. (a) Sum of gates set on ground-state band transitions, (b) gate set on 195-keV transition, (c) gate set on 222-keV transition, (d) gate set on 372-keV transition. The positions of ground-state band transitions are marked with dashed lines. The positions of the unplaced transitions at 195, 222, and 372 keV are marked with dotted lines.

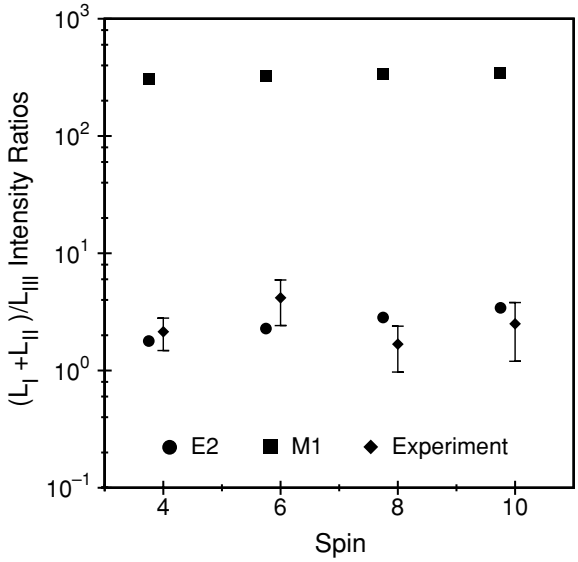

FIG. 10. Comparison of experimentally determined L conversion line intensity ratios with those expected for $E2$ and $M1$ transition types.

gate sum we clearly see all the ground-state band members reproduced. We also observe significant intensity in a wide region around 470 keV, suggesting that this may be the energy of the $20^+ \rightarrow 18^+$ transition. However, with no clear peak visible in the recoil gated spectrum we prefer not to make this assignment. Of the unplaced transitions, only the 222-keV transition appears in the ground-state band gate sum. From panel (c) of Fig. 9 it is clear that these few counts arise through coincidence with the 397- and 434-keV transitions. With the available statistics it is certainly not possible to fit the unplaced transitions into a level scheme.

A useful property of the internal conversion process is the sensitivity of internal conversion coefficients (ICCs) to transition type. Across the observed energy range, the intensity ratios of the combined $L1 + L2$ components to the $L3$ component of each transition are strongly dependent on the transition type involved. Shown in Fig. 10 are the ratios measured for the electron line components in the recoil gated electron spectrum together with those expected for $E2$ and $M1$ transition types. The large difference between the ratios expected for $M1$ and $E2$ transition types allows the nature of the ground-state band members to be firmly established as $E2$. Note that the ratios are only weakly dependent on the efficiency of the SACRED spectrometer as the lines in question are only 7 keV apart. From the coincidence of the transitions, their confirmed $E2$ character and also their similarities to the transition energies observed in ^{254}No, we conclude that we have indeed observed the ground-state band of ^{250}Fm from the $4^+ \rightarrow 2^+$ transition up to the $18^+ \rightarrow 16^+$ transition and confidently assign spins and parities.

D. Electron spectra

In addition to the ground-state band, an unplaced 113-keV transition without a counterpart in the γ-ray spectra is found.

The peak lies between the L and M components from the $4^+ \rightarrow 2^+$ transition and is labeled with a question mark in Fig. 4. The unplaced 113-keV transition should be visible in the γ-ray spectra with an intensity dependent on its transition type. Unfortunately a γ-ray peak of energy 113 keV would lie beneath the combined $K_{\alpha 2} + K_{\alpha 3}$ Fm x-ray line. Despite this, comparison of the measured intensity ratio of the $K_{\alpha 1}$ line with the combined $K_{\alpha 2} + K_{\alpha 3}$ line, together with knowledge of the intensity of the unknown peak in conversion electrons, allows us to set a lower limit on the ICC involved. This limit is derived from a calculated maximum number of counts in the $K_{\alpha 2} + K_{\alpha 3}$ Fm x-ray line that can arise from the 113-keV transition while maintaining consistency with the number of counts in the $K_{\alpha 1}$ line. From the measured ratio of the number of counts in the $6^+ \rightarrow 4^+$ ground-state band transition in the γ-ray and conversion electron spectra and correcting for the energy dependence of the ICC and efficiency of the devices, we obtain a lower limit of $\alpha_{113} = 0.7$. For transition types $E1$, $E2$, and $M1$, the published ICCs [39] are 0.1, 15.3, and 8.0, respectively. The limit effectively rules out electric dipole transitions only.

A prominent feature of the recoil tagged electron spectrum is the large background at low energies. Panel (a) of Fig. 11 shows the total recoil tagged electron spectrum, In this spectrum, ground-state band transitions are seen sitting on a background peaking at around 90 keV. Shown in panel (c) is the corresponding recoil decay tagged spectrum. The background is clearly present, indicating that it does indeed originate from ^{250}Fm. Following the procedure outlined in [26], we want to establish that the background observed is of nuclear origin and can be attributed to decay by means of high-K bands that collect part of the intensity and are likely to channel it through highly converted low-energy $M1$ transitions. To do that we need two key observables. As the population of states is expected to occur in the spin region around 14–20, the average multiplicity of electrons in the ground-state band and in the high-K $M1$ band will be different. An estimate of this multiplicity can be obtained from a comparison of the observed intensities in the spectra in which only a single electron has been observed (fold 1) with those in the spectra in which all electron multiplicities have been allowed. The upper two panels of Fig. 11 show this comparison. It is clear that the condition of fold 1 favors the ground-state band with its lower multiplicity. It is useful to define a quantity R equal to the ratio of the measured intensity when only fold 1 events are incremented to the measured intensity when all folds are allowed. For the L components of the ground-state band we measure the value $R_{\text{exp}} = 0.74 \pm 0.13$. This value is consistent with the value $R_{\text{theo}} = 0.83 \pm 0.02$ expected for the visible ground-state band cascade when the energy dependence of the ICC and the efficiency of the SACRED spectrometer are taken into account. This value corresponds to an average multiplicity of 2.2 ± 0.1 for electrons in the visible part of the ground-state band.

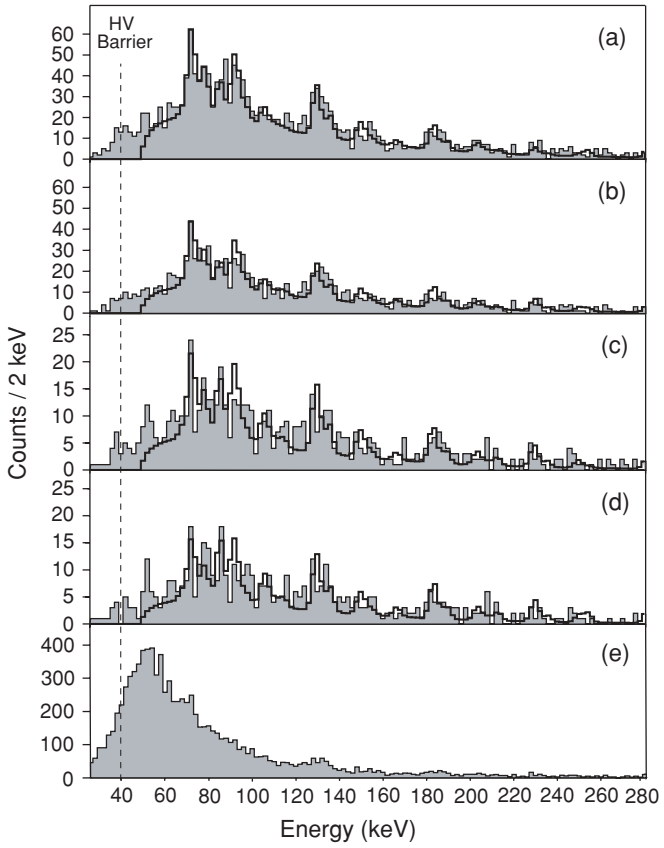

FIG. 11. (a) Recoil tagged electron spectrum including all multiplicities, (b) recoil tagged electron spectrum including fold 1 events only, (c) recoil decay tagged electron spectrum including all multiplicities, (d) recoil decay tagged electron spectrum including fold 1 events only, (e) electron spectrum taken in random coincidence.

The electron coincidence spectra suggest that the unplaced transition at 113 keV is in coincidence with the observed ground-state band. If this is the case then, owing to the large probability of internal conversion at 113 keV, the transition must affect the average multiplicity. If the transition feeds into the ground-state band above the transitions observed in the electron spectra, then the visible ground-state band cascade can be considered to contain an additional transition. If one assumes the transition to be fed roughly equal to transitions in the ground-state band then a value $R_{\text{theo}} = 0.78 \pm 0.02$ is expected. The transition is likely to be either $E2$ or $M1$ in character. To within errors, the expected values are not affected by that assumption. It is interesting to note that the predicted value of R is closer to the experimentally measured value if the unplaced 113-keV transition and ground-state band are assumed to be in coincidence. The final placement of this transition will require γ-electron coincidences to be measured in the future.

In the case of the background we measure a ratio $R_{\text{exp}} = 0.59 \pm 0.03$. Assuming the background arises from strongly converted $M1$ transitions we expect a value $R_{\text{theo}} = 0.62 \pm 0.05$ for a cascade of six transitions and $R_{\text{theo}} = 0.57 \pm 0.05$ for a cascade of seven transitions. We thus obtain the average multiplicity of electrons in the background as 6.5 ± 0.5 through interpolation.

We can gain insight into the proportion of ^{250}Fm residues decaying by means of the ground-state band from the number of observed ground-state band γ-rays as a function of the number of recoils. To avoid complications arising from

the position of the polygonal time-of-flight gate, we use the number of recoils passing the gate that are correlated with an α decay occurring within three half-lives. In the γ-ray experiment we observe 4652 such recoils. From the assumption of a 90% α-decay branch and correcting for the efficiency of JUROSPHERE IV and the relevant ICC, we expect 55 ± 2 and 122 ± 2 counts in the $6^+ \rightarrow 4^+$ and $8^+ \rightarrow 6^+$ γ-ray peaks, respectively. The observed peak areas are $A_{6^+\rightarrow 4^+} = 24 \pm 6$ counts and $A_{8^+\rightarrow 6^+} = 61 \pm 9$ counts. The values allow the proportion of ^{250}Fm nuclei decaying through the $6^+ \rightarrow 4^+$ and $8^+ \rightarrow 6^+$ transitions to be determined as $R_{6^+\rightarrow 4^+} = (43 \pm 10)\%$ and $R_{8^+\rightarrow 6^+} = (50 \pm 8)\%$. In the conversion electron experiment we observe 2440 correlated recoils and thus expect 406 ± 60 counts and 263 ± 40 counts in the L components of the $4^+ \rightarrow 2^+$ and $6^+ \rightarrow 4^+$ transitions, respectively. We observe $A_{4^+\rightarrow 2^+} = 138 \pm 15$ and $A_{6^+\rightarrow 4^+} = 95 \pm 12$ counts corresponding to fractions of the ^{250}Fm nuclei decaying through the transitions equal to $R_{4^+\rightarrow 2^+} = (53 \pm 10)\%$ and $R_{6^+\rightarrow 4^+} = (24 \pm 7)\%$. We conclude that roughly 50% of the decay passes through the ground-state band. Finally, we must show that the background is not of another physical origin. In [26] we have already shown that the spectral response of the SACRED spectrometer cannot be responsible for the background. An electron spectrum gated far off the prompt recoil-electron time peak is shown in panel (e) of Fig. 11 and shows a shape characteristic of a δ-electron spectrum. It clearly peaks near the barrier voltage and exhibits an exponential drop at higher energies. This spectral shape is clearly different from that shown in the other panels, demonstrating that the background does not arise from atomic processes such as collisions between beam particles and atoms in the gas.

As with the γ-ray data it is possible to gain insight into the nature of unknown transitions by use of electron-electron coincidence analysis. Again the level of statistics is at the useful limit, and additional complications arise from the presence of the nuclear background. As the ground-state band electron lines sit on top of the background, it is unclear whether counts seen in gated spectra arise from coincidences with ground-state band or the background electrons. Shown in panel (a) of Fig. 12 is the total recoil gated electron spectrum of Fig. 4. Shaded regions indicate the gates used to produce subsidiary panels (b)–(d). Panel (b) shows the spectrum produced by summing the gates on all the ground-state band transition lines (gray-shaded areas). No gate was set on the M conversion line from the $4^+ \rightarrow 2^+$ transition as the line is contaminated by the unplaced 113-keV transition. The spectrum shows counts in the positions corresponding to the ground-state band lines, further evidence of the ground-state bands' mutual coincidence. The spectrum also includes counts in the region of the uncontaminated line from the 113-keV transition, suggesting that it is in coincidence with the ground-state band. In panel (c) we show a sum of gates set on regions of clean background. The gating regions were chosen to avoid contamination from the ground-state band. The expected locations of K conversion lines from higher-lying transitions were also avoided. No gate was set on the region below 50 keV in order to avoid complications arising from the electrostatic barrier. The intensity distribution is similar to

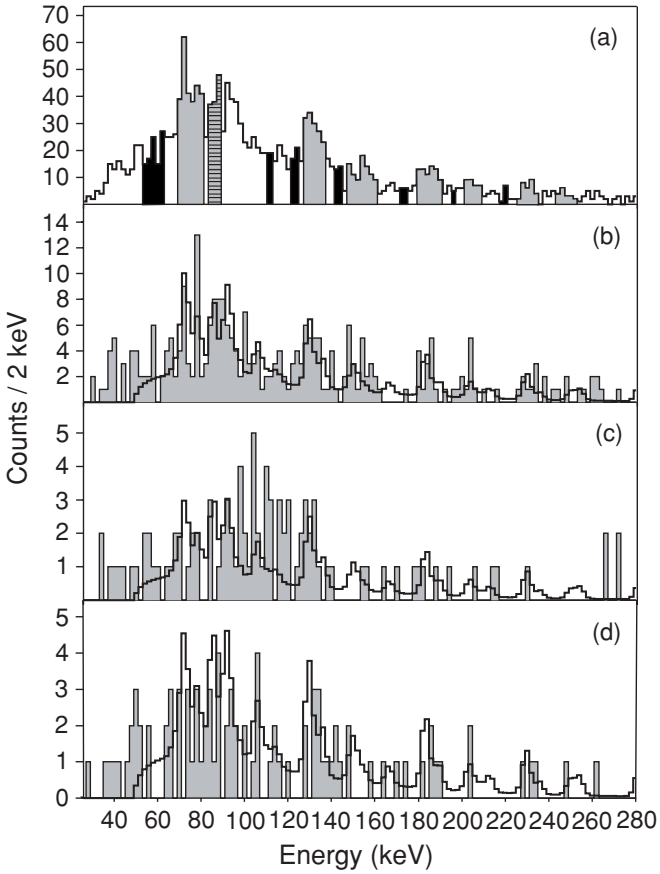

FIG. 12. (a) Total recoil gated electron spectrum; gray areas mark gates placed on ground-state transition lines. A gate was not placed on the M conversion line from the $4^+ \rightarrow 2^+$ transition as the line is contaminated by the unplaced 113-keV transition. Black areas mark gates set on areas of clean background, and the hatched region marks the gate set on the 113-keV transition. (b) Sum of gates set on all ground-state band transition lines. (c) Sum of gates set on regions of clean background. (d) Spectrum gated on the 113-keV transition. In all the panels a fitted simulation spectrum (solid curve) is included to guide the eye.

that of the background observed in the singles data. Intensity is observed in the region of the $6^+ \rightarrow 4^+$ L conversion line. However, the poor statistics prevent us from drawing conclusions about coincidence between the background and ground-state band. In panel (d) we show a spectrum gated on the 113-keV transition. It brings back the ground-state band transitions from $4^+ \rightarrow 2^+$ up to $10^+ \rightarrow 8^+$, indicating that this transition feeds into the top half of the band.

IV. DISCUSSION

A. Level scheme

The proposed level scheme is shown in Fig. 13. The next transition of the ground-state band is expected around 470 keV. Indeed two weak peaks are observed at 470 and 476 keV. The ground-state band gate sum of Fig. 9 appears to favor 470 keV. However, at the present level of statistics it is

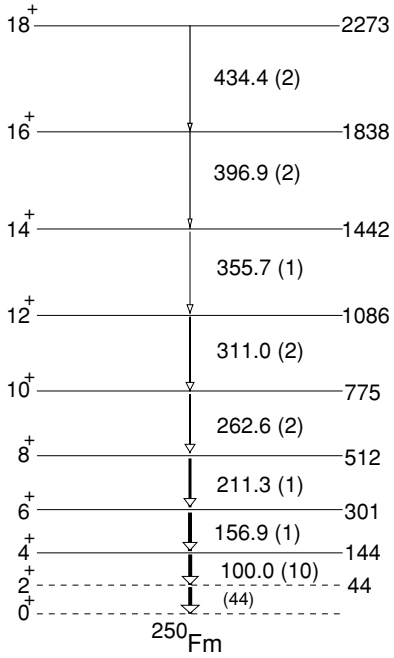

FIG. 13. The proposed level scheme of ^{250}Fm.

not possible to decide which line represents the continuation of the band. None of the other observed peaks in the γ-ray or conversion electron spectra can be firmly placed and are not shown in Fig. 13.

B. Deformation

The observation of a rotational ground-state band indicates that ^{250}Fm is deformed. The $B(E2)$ values of rotors are related to the 2^+ level energies by empirical formulas given in [40–42]. The energy of the 2^+ state is not measured with γ rays as the ICCs at such energies are too large, and it is not measured with conversion electrons as it is not sufficiently energetic to pass the −40-kV electrostatic barrier. The energy can, however, be deduced by use of a method detailed in [43]. In Fig. 14 we plot the kinematic moment of inertia $J^{(1)} = \{[\hbar^2(2I-1)]/[E_\gamma(I)]\}$ and dynamic moment of inertia $J^{(2)} = \{4\hbar^2/[E_\gamma(I) - E_\gamma(I-2)]\}$ as a function of rotational frequency. The Harris parametrization

$$J^{(1)} = J_0 + J_1\omega^2, \quad (1)$$

$$J^{(2)} = J_0 + 3J_1\omega^2, \quad (2)$$

with $\hbar\omega = E_\gamma/2$ produces good fits to the data. From extrapolation of the fits and the relation

$$I = J_0\omega + J_1\omega^3 + \tfrac{1}{2}, \quad (3)$$

we estimate the energies of the transitions from the 2^+ and 4^+ states as (44 ± 1) keV and (101 ± 1) keV. The latter value is in agreement with the value (100 ± 1) keV obtained from electron spectroscopy. From the empirical relations we thus obtain $B(E2; 2^+ \rightarrow 0^+) = 375 \pm 50$ W.u. and a quadrupole deformation parameter of $\beta_2 = 0.28 \pm 0.02$.

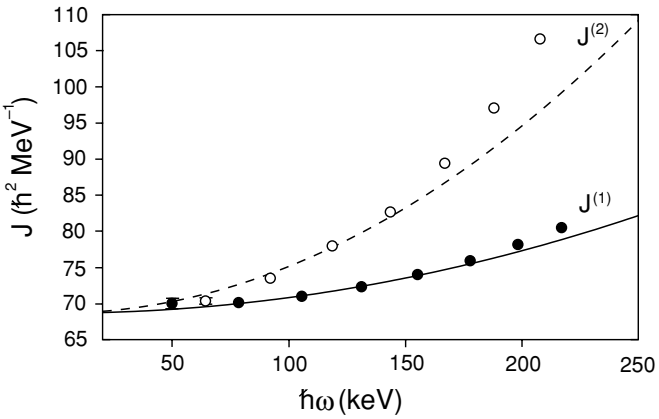

FIG. 14. Kinematic and dynamic moments of inertia for the ground-state band. The solid and dashed lines are fits to the data by use of Eqs. (1) and (2).

V. MODEL CALCULATIONS

The CRHB theory [44,45] has been used for the study of rotational and deformation properties of the observed band. The calculations were performed with two parametrizations of the RMF Lagrangian (NL1, NL3) for the particle-hole channel and with the D1S Gogny force for the particle-particle channel in the manner described in Ref. [15]. In addition, approximate particle-number projection by means of the Lipkin-Nogami method has been employed. The calculated quadrupole deformations ($\beta_2 \approx 0.31$ for NL1 and $\beta_2 \approx 0.29$ for NL3) are in good agreement with experimental estimates. Calculated kinematic and dynamic moments of inertia are compared with experiment in Fig. 15. Experimental data are well described by the calculations, especially with NL3 parametrization: The calculation with NL1 somewhat overestimates $J^{(1)}$ and $J^{(2)}$ at high frequencies. Gradual alignment of $i_{13/2}$ protons and $j_{15/2}$

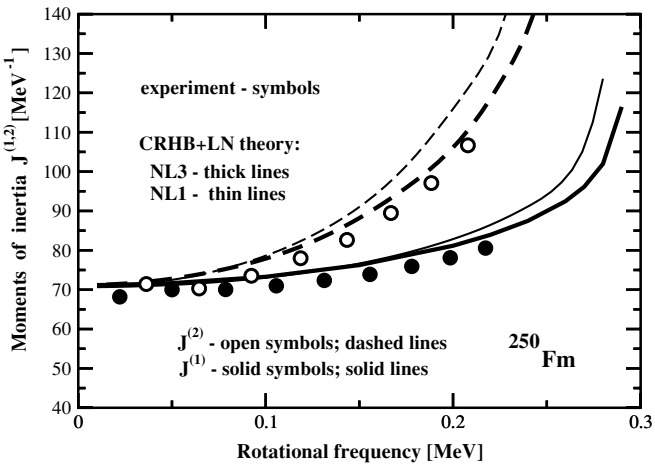

FIG. 15. Experimental and calculated kinematic and dynamic moments of inertia of the ground-state band in ^{250}Fm. The results of the calculations with NL1 and NL3 parametrizations of the RMF Lagrangian are shown only up to a rotational frequency at which a sharp band crossing takes place.

neutrons and the decrease of pairing are responsible for the rise of kinematic and dynamic moments of inertia with increasing rotational frequency. In both parametrizations, sharp paired band crossing takes place at $\omega \sim 0.29$ MeV.

VI. CONCLUSIONS

For the first time, in-beam γ-ray and conversion electron spectroscopy have been applied to observe the nucleus ^{250}Fm. Rotational ground-state band transitions have been observed from spin $6^+ \rightarrow 4^+$ up to $18^+ \rightarrow 16^+$ by use of γ rays, and from $4^+ \rightarrow 2^+$ up to $10^+ \rightarrow 8^+$ by use of conversion electrons. By extrapolation of Harris fits to the kinematic and dynamic moments of inertia, we estimate the energies of the unobserved $2^+ \rightarrow 0^+$ transition and thus obtain a quadrupole deformation of $\beta_2 = 0.28 \pm 0.02$. From the sensitivity of internal conversion coefficients to transition type, we confirm the $E2$ nature of the ground-state band. Additional transitions are observed at 195, 222, and 372 keV in γ rays and at 113 keV in conversion electrons. The construction of γ-γ and electron-electron matrices allows the coincidence of the ground-state band transitions to be confirmed. The statistics obtained do not allow the additional transitions to be placed in a level scheme. In the conversion electron spectra we observe a background of apparent nuclear origin peaking around 90 keV. The background is measured to have a higher average multiplicity than transitions in the ground-state band. This is consistent with decay by means of high-K bands that collect a part of the decay intensity. Measurements made on the ground-state band transitions indeed indicate that the decay of a significant fraction of the initially populated states does not promptly feed into the ground-state band. We measure the α-decay half-life of ^{250}Fm to be (30.4 ± 1.5) min.

It is encouraging to find good agreement between theory and experiment for the observed moment of inertia in the experimentally probed range of spins. Although an extension of the bands past this first upbend would be highly desirable, the narrow energy window in which the excitation function produces ^{250}Fm with sufficient cross section precludes such an extension in the present generation of experiments. However, the most sensitive probe of model calculations capable of describing the observed upbend will be the successful description of bands in the neighboring odd-mass systems. Such experiments are currently planned.

ACKNOWLEDGMENTS

We thank the staff at the University of Jyväskylä Accelerator Laboratory for their expertise and dedication. This work has been supported by the European Union Fifth Framework Programme "Improving Human Potential - Access to Research Infrastructure," contract no. HPRI-CT-1999-00044, EXOTAG (contract no. HPRI-1999-CT-50017), and by the Academy of Finland under the Finnish Centre of Excellence Programme 2000-2005 (project no. 44875, Nuclear and Condensed Matter Physics Programme at JYFL). R.-D. Herzberg gratefully acknowledges an EPSRC Advanced Research Fellowship. The work of A. V. Afanasjev was supported by the U.S. Department of Energy grant DE-F05-96ER-40983. A. Chatillon gratefully acknowledges a European Community Marie Curie Fellowship. We would also like to thank the EPSRC-IN2P3 Loanpool for the Ge detectors that comprise JUROSPHERE IV.

[1] A. Sobiczewski, F. A. Gareev, and B. N. Kalinkin, Phys. Lett. **22**, 500 (1966).
[2] V. A. Chepurnov, Yad. Fiz. **6**, 955 (1967).
[3] S. G. Nilsson *et al.*, Nucl. Phys. **A131**, 1 (1969).
[4] S. G. Nilsson *et al.*, Nucl. Phys. **A115**, 545 (1968).
[5] Z. Patyk, A. Sobiczewski, P. Armbruster, and K.-H. Schmidt, Nucl. Phys. **A491**, 267 (1989).
[6] Z. Patyk and A. Sobiczewski, Nucl. Phys. **A533**, 132 (1991).
[7] P. Möller and J. R. Nix, J. Phys. G: Nucl. Part. Phys. **20**, 1681 (1994).
[8] P. Möller and J. R. Nix, Nucl. Phys. **A549**, 84 (1992).
[9] R. Smolanczuk, Phys. Rev. C **56**, 812 (1992).
[10] S. Cwiok, J. Dobaczewski, P.-H. Heenen, P. Magierski, and W. Nazarewicz, Nucl. Phys. **A611**, 211 (1996).
[11] K. Rutz, M. Bender, T. Burvenich, T. Schilling, P. G. Reinhard, J. A. Maruhn, and W. Greiner, Phys. Rev. C **56**, 238 (1997).
[12] M. Bender, K. Rutz, P.-G. Reinhard, J. A. Maruhn, and W. Greiner, Phys. Rev. C **60**, 034304 (1999).
[13] G. A. Lalazissis, M. M. Sharma, P. Ring, and Y. K. Gambhir, Nucl. Phys. **A608**, 202 (1996).
[14] M. Bender, P.-H. Heenen, and P.-G. Reinhard, Rev. Mod. Phys. **75**, 121 (2003).
[15] A. V. Afanasjev, T. L. Khoo, S. Frauendorf, G. A. Lalazissis, and I. Ahmad, Phys. Rev. C **67**, 024309 (2003).
[16] S. Hofmann *et al.*, Z. Phys. A **354**, 229 (1996).
[17] Y. T. Oganessian *et al.*, Phys. Rev. Lett. **83**, 3154 (1999).
[18] Y. T. Oganessian *et al.*, Phys. Rev. C **69**, 021601(R) (2004).
[19] Y. T. Oganessian *et al.*, Phys. Rev. C **63**, 011301(R) (2000).
[20] K. Morita *et al.*, J. Phys. Soc. Jpn. **73**, 2593 (2004).
[21] R. R. Chasman and I. Ahmad, Phys. Lett. **B392**, 255 (1997).
[22] R. R. Chasman *et al.*, Rev. Mod. Phys. **49**, 833 (1977).
[23] M. Leino *et al.*, Eur. Phys. J. A **6**, 63 (1999).
[24] R.-D. Herzberg *et al.*, Eur. Phys. J. A **15**, 205 (2002).
[25] P. Reiter *et al.*, Phys. Rev. Lett. **84**, 3542 (2000).
[26] P. A. Butler *et al.*, Phys. Rev. Lett. **89**, 202501 (2002).
[27] R.-D. Herzberg *et al.*, Phys. Rev. C **65**, 014303 (2001).
[28] P. T. Greenlees *et al.*, Eur. Phys. J. A **20**, 87 (2004).
[29] M. Leino *et al.*, Nucl. Instrum. Methods Phys. Res. B **99**, 653 (1995).
[30] M. Leino, Nucl. Instrum. Methods Phys. Res. B **126**, 320 (1997).
[31] U. Friebel *et al.*, in *Proceedings of the Fifth Annual Conference of the International Nuclear Target Development Society*.
[32] T. L. Morgan *et al.*, in *Proceedings of the Tenth World Conference of the International Nuclear Target Development Society*.
[33] E. S. Paul *et al.*, Phys. Rev. C **51**, 78 (1995).

[34] R. S. Simon *et al*., Z. Phys. A **325**, 197 (1986).
[35] P. A. Butler *et al*., Nucl. Instrum. Methods Phys. Res. A **381**, 433 (1996); H. Kankanpää *et al*., *ibid*. **534**, 503 (2004).
[36] A. Artna-Cohen, Nucl. Data Sheets **84**, 901 (1998).
[37] M. E. Leino, S. Yashita, and A. Ghiorso, Phys. Rev. C **24**, R2370 (1981).
[38] Y. A. Akovali, Nucl. Data Sheets **84**, 1 (1998).
[39] F. Rosel *et al*., At. Data Nucl. Data Tables **21**, 91 (1978).
[40] L. Grodzins, Phys. Lett. **2**, 88 (1962).
[41] S. Raman *et al*., At. Data Nucl. Data Tables **42**, 1 (1989).
[42] W. Nazarewicz and I. Ragnarsson, *Handbook of Nuclear Properties* (Clarendon, Oxford, 1996), p. 97.
[43] J. E. Draper *et al*., Phys. Rev. C **42**, R1791 (1990); J. Becker *et al*., *ibid*. **46**, 889 (1992); G. Hackman *et al*., Phys. Rev. Lett. **79**, 4100 (1997).
[44] A. V. Afanasjev, J. König, and P. Ring, Phys. Rev. C **60**, 051303(R) (1999).
[45] A. V. Afanasjev, P. Ring, and J. König, Nucl. Phys. **A676**, 196 (2000).